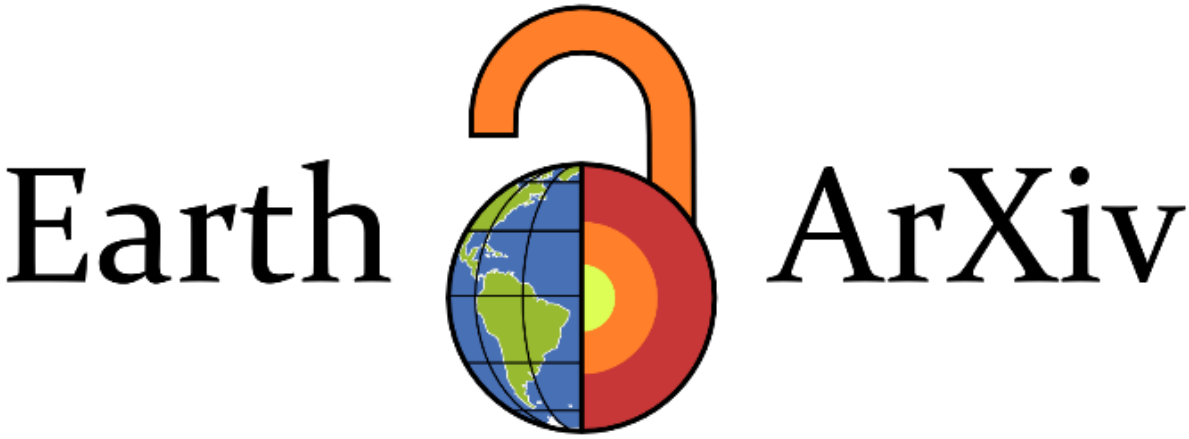


Title:
Estimation of Near-Surface Density using Vertical Gravity Gradients in Central and Western Japan

Ryuichi Nishiyama*
*Earthquake Research Institute, The University of Tokyo, Japan
(r-nishi@eri.u-tokyo.ac.jp)

Peer review status:
This is a non-peer-reviewed preprint submitted to EarthArXiv.

# Estimation of Near-Surface Density using Vertical Gravity Gradients in Central and Western Japan

Ryuichi Nishiyama*

## Abstract

The Vertical Gravity Gradient (VGG), derived from the difference between terrestrial and airborne gravity data, highlights shallow density contrasts. We estimated the near-surface density structure of Central and Western Japan using VGGs derived from terrestrial data within 3 km of airborne flight lines. We constructed an inversion model on a 1/7-degree grid to estimate surface density and a regional VGG trend, imposing spatial continuity constraints on the trend. Hyperparameters were determined by minimizing the Akaike Bayesian Information Criterion (ABIC). The resulting model clearly identifies low-density zones in major plains, such as Kanto and Echigo, and distinct low-VGG anomalies along the Itoigawa-Shizuoka Tectonic Line (western margin of the Fossa Magna) and the Osaka-Lake Biwa region. The estimated surface density showed a weak correlation with seismic S-wave velocity models.

.

## 1 Introduction

Gravity surveys have long been a fundamental tool for investigating subsurface density structures. Conventionally, these studies rely on gravity anomalies (e.g. Bouguer anomalies) to infer geological features. However, gravity anomalies are integral fields that decay with the square of the distance ($1/r^2$) from the source. Consequently, the signals observed at the surface are often dominated by long-wavelength components originating from deep structures, such as the Moho discontinuity or subducting slabs. This makes it challenging to isolate and resolve short-wavelength signals associated with near-surface geological structures, such as sedimentary basins and upper crustal faults.

* Earthquake Research Institute, The University of Tokyo, Japan (r-nishi@eri.u-tokyo.ac.jp)

To overcome this limitation, the Vertical Gravity Gradient (VGG) has gained attention as a superior indicator for shallow exploration. Since the gravity gradient decays with the cube of the distance ($1/r^3$), it effectively acts as a high-pass filter that surpasses deep-seated trends and highlights shallow density contrasts. While VGG is commonly used in resource exploration, its application to regional-scale crustal modeling has been limited by the scarcity of direct gradiometer measurements.

In the context of the Japanese Islands, Nawa et al. (1997) [1] compiled a comprehensive density map using a nationwide terrestrial gravity database. While their work provided a crucial baseline for understanding the crustal structure of Japan, their estimation based on Bouguer anomalies inherently included significant influences from deep-seated tectonics.

In this study, we propose a method to estimate the near-surface density structure of Central and Western Japan by utilizing the Vertical Gravity Gradient. Instead of using expensive gradiometers, we derive VGG by calculating the difference between terrestrial gravity data and the recently released airborne gravity data provided by the Geospatial Information Authority of Japan (GSI). By exploiting the altitude difference between land and air measurements, we extract gradient information empirically. We applied an inversion analysis to this derived VGG dataset to reconstruct the average density structure up to a depth of 8 km, demonstrating the performance of this approach for delineating sedimentary basins and major tectonic lines.

# 2 Data and Processing

## 2.1 Terrestrial Gravity Data

To ensure sufficient spatial density and coverage over the study area, we integrated terrestrial gravity data from four major databases available in Japan. The datasets used in this study are:

1. Gravity data provided by the Geospatial Information Authority of Japan (GSI) (13,978 points) [2]
2. Gravity Database of Japan, DVD Edition, published by the Geological Survey of Japan (GSJ), AIST (173,365 points) [3]
3. Gravity Database of the Kanazawa University (19,894 points) [4]

4. Gravity Database of Southwest Japan and Gravity Database of Japan (combining the 2001 and 2011 versions; 139,907 points) [5,6]

We performed data screening to ensure quality, selecting only those stations with complete and reliable records of latitude, longitude, elevation and absolute gravity values. A total of 344,520 terrestrial gravity stations were utilized for the analysis. The spatial distribution of these stations is illustrated in Figure 1(a).

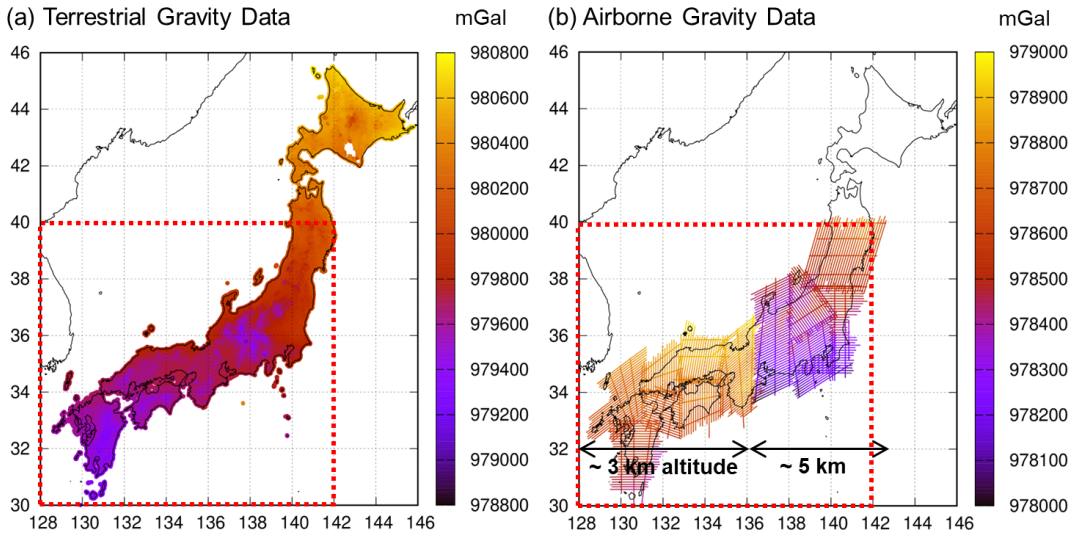


**Figure 1** (a) Terrestrial and (b) airborne gravity dataset employed in this study. Red rectangles denote the study area of this VGG analysis.

## 2.2 Airborne Gravity Data

For the airborne component, we utilized the "Airborne Gravity Data" released by the Geospatial Information Authority of Japan (GSI) in March 2024 [7]. This comprehensive dataset was acquired through extensive surveys conducted between 2019 and 2023, covering almost all of Japan.

The data is organized by survey blocks and individual flight lines. Each data record provides the observation time (UTC), latitude, longitude, ellipsoidal height, and absolute gravity value. A critical parameter for our VGG estimation is the flight altitude, which varies depending on the survey region to accommodate terrestrial topography and airspace restrictions.

In our study area (limited to regions south of 40°N), the design flight altitudes are broadly categorized into two levels: approximately 3,000 m in Western Japan and 5,000 m in Eastern and Central Japan. Specifically, we used data from the following survey blocks:

- 3,000 m altitude: CB02, CG01, CG02, CG03, KY01, KY02, and KY03.
- 5,000 m altitude: CB01, KT01, KT02, KT03, and TH02.

The spatial distribution of these flight lines and the observed gravity values used in this study are visualized in Figure 1(b). Note here that the gravity values provided in the dataset are absolute gravity at the flight altitude and are not Bouguer anomalies.

## 2.3 Derivation of Vertical Gravity Gradients (VGG)

We derived the VGG directly from the difference between terrestrial and airborne gravity datasets. For each of the 344,520 terrestrial gravity stations, we searched for airborne data points within a horizontal distance of 3km. If airborne data existed within this radius, we selected only the single point with the shortest horizontal distance. Through this selection process, a total of 247,633 valid terrestrial-airborne pairs were established for the analysis.

A critical challenge in calculating the precise vertical distance ($dz$) between these pairs lies in the different height systems used in the datasets. The terrestrial gravity data are provided with elevations relative to the mean sea level (orthometric height, $H_{land}$), whereas the airborne gravity data are referenced to the GRS80 ellipsoid (ellipsoidal height, $h_{air}$). Since subsequent processing steps, such as terrain correction, are conducted based on orthometric heights, we unified the height system by converting the airborne ellipsoidal heights into orthometric heights ($H_{air}$). This conversion is given by:

$$H_{air} = h_{air} - N,$$

where $N$ is the geoid height.

We obtained $N$ using GSIGEO2024beta (Geoid 2024 Japan and its surroundings, Trial Version [8]), the latest gravimetric geoid model released by GSI in March 2024. This model is constructed by integrating satellite, airborne, terrestrial, and marine gravity data. The model achieves high accuracy, with a standard deviation of geoid height differences evaluated at approximately 2.8 cm.

Using the unified orthometric heights, we calculated the vertical gravity gradient ($\gamma_{\mathrm{obs}}$) for each pair as:

$$\gamma_{\mathrm{obs}} = \frac{g_{land} - g_{air}}{H_{air} - H_{land}},$$

where $g_{land}$ and $g_{air}$ are the absolute gravity values at the terrestrial and airborne stations, respectively. Figure 2 presents the distribution of $\gamma_{\mathrm{obs}}$ calculated over the Japanese Islands.

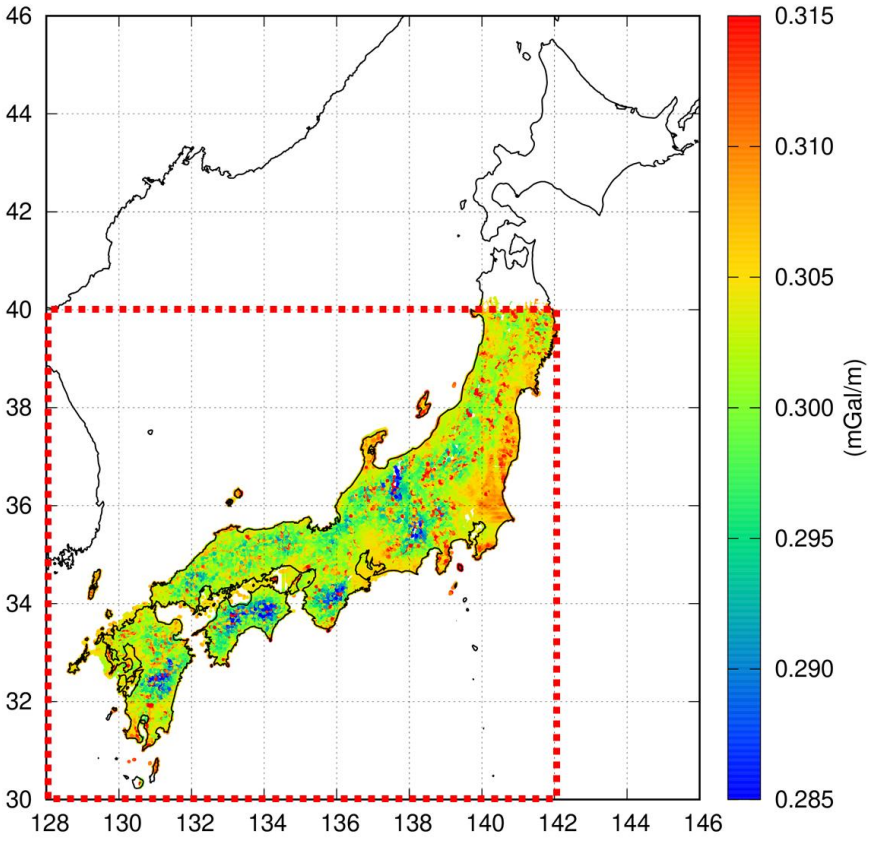


**Figure 2** Vertical Gravity Gradient (VGG) distribution over the Japan Islands, which is calculated from the difference of the terrestrial and airborne gravity measurements data. Red rectangles denote the study area of this VGG analysis.

# 3 Method

## 3.1 Model Formulation

The observed vertical gravity gradient, $\gamma_{\mathrm{obs}}$, represents a superposition of signals from various subsurface and surface mass distributions. To isolate the near-surface density effects, we model the observed VGG at the i-th data point as the sum of three components: (1) a regional trend originating from deeper crustal structures, (2) the gravitational effect of local surface topography, and (3) the gravitational effect of seawater. The observation equation is expressed as:

$$\gamma_{\mathrm{obs},i} = \gamma_{\mathrm{regional},i} + \rho_k A_{\mathrm{topo},i}(\delta) + \rho_{\mathrm{water}} A_{\mathrm{water},i}(\delta) + \epsilon_i,$$

where $\epsilon_i$ represents the observation error. The study area is discretized into a uniform grid with a spatial resolution of $1/7\,^\circ \times 1/7\,^\circ$. Within the k-th grid cell, we assume that the surface density $\rho_k$ is constant. Furthermore, to capture the spatially varying nature of the regional field, we parameterize $\gamma_{\mathrm{regional}}$ within each cell as a local planar trend:

$$\gamma_{\mathrm{regional},i} = \alpha_k(x_i - x_{c,k}) + \beta_k(y_i - y_{c,k}) + C_k,$$

where $(x_i, y_i)$ are the coordinates of the observation point, and $(x_{c,k}, y_{c,k})$ is the center of the k-th grid cell. Consequently, for each grid cell, there are four unknown parameters to be estimated: the density $\rho_k$ and the trend coefficients $\alpha_k, \beta_k, C_k$. Here, $A_{\mathrm{topo},i}(\delta)$ and $A_{\mathrm{water},i}(\delta)$ denote the gravitational responses per unit density for topography and seawater, respectively. Both terms depend on the assumed thickness (depth) of the surface density contrast layer, $\delta$.

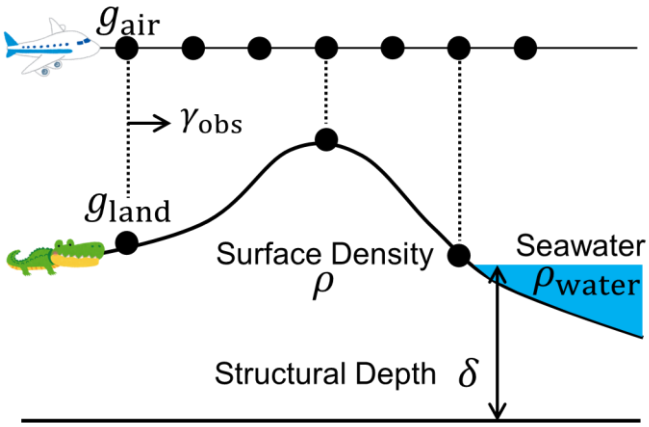


**Figure 3** Schematic illustration of the VGG observation geometry and model parameterization. The observed vertical gravity gradient ($\boldsymbol{\gamma_{\mathrm{obs}}}$) is derived from the difference between terrestrial gravity ($\boldsymbol{g_{\mathrm{land}}}$) and airborne gravity ($\boldsymbol{g_{\mathrm{air}}}$). The model assumes a constant surface density ($\boldsymbol{\rho}$) for the topography extending down to a structural depth ($\boldsymbol{\delta}$), while accounting for the known density of seawater ($\boldsymbol{\rho_{\mathrm{water}}}$).

### 3.2 Computation of Gravitational Responses

We computed the gravitational responses $A_{\mathrm{topo},i}(\delta)$ and $A_{\mathrm{water},i}(\delta)$ by numerically integrating the gravitational attraction of mass prisms derived from digital elevation/bathymetry models. For land topography, we used the Copernicus GLO-90 Digital Elevation Model [9]. For bathymetry, we employed the GEBCO 2024 Grid [10]. The numerical integration was performed using a cylindrical segmentation method (e.g. Hofmann-Wellenhof & Moritz, 2006 [11]) to accurately account for the near-field geometry around each computation point. Specifically, both responses are calculated by assuming a constant density extending from the surface (or sea surface) down to the depth $\delta$.

### 3.3 Bayesian Inversion Scheme

We formulated the estimation of the unknown parameters vector $\mathbf{m} = (\alpha_1, \beta_1, C_1, \rho_1, \cdots, \alpha_m, \beta_m, C_m, \rho_m)^{\mathrm{T}}$ as a linear inverse problem:

$$\mathbf{d} = \mathbf{G}(\delta)\,\mathbf{m} + \mathbf{e}$$

where $\mathbf{d}$ is the data vector containing VGG observations corrected for the known seawater effect (calculated with $\rho_{\mathrm{water}} = 1000\ \mathrm{kg\ m^{-3}}$), and $\mathbf{G}(\delta)$is the design matrix, which varies depending on the assumed depth parameter $\delta$. To mitigate the ill-posedness of the inversion and to obtain a physically plausible solution, we introduced a smoothness constraint on the regional trend parameters. We assume that the regional VGG field varies continuously across adjacent grid cells. This constraint is implemented by minimizing the discrepancy of the planar trends at the boundaries of neighboring cells, written in matrix form as:

$$\mathbf{Lm} = \mathbf{0}$$

where $\mathbf{L}$ is the roughness operator matrix.

The optimal model parameters $\widehat{\mathbf{m}}$ are obtained by minimizing the following objective function $U(\mathbf{m})$:

$$U(\mathbf{m}) = \|\mathbf{d} - \mathbf{G}(\delta)\,\mathbf{m}\|^2 + \lambda^2\|\mathbf{Lm}\|^2$$

where $\lambda$ is a regularization weight that controls the trade-off between data fitting and model smoothness. Minimizing $U(\mathbf{m})$ with respect to $\mathbf{m}$ yields the explicit least-squares solution:

$$\widehat{\mathbf{m}} = \left(\mathbf{G}(\delta)^{\mathrm{T}}\mathbf{G}(\delta) + \lambda^2\mathbf{L}^{\mathrm{T}}\mathbf{L}\right)^{-1}\mathbf{G}(\delta)^{\mathrm{T}}\mathbf{d}$$

### 3.4 Optimization of Hyperparameters and Error Estimation

The inversion involves two key hyperparameters: the regularization weight $\lambda$ and the structural depth parameter $\delta$. We determined the optimal combination of these parameters objectively based on the Akaike Bayesian Information Criterion (ABIC) [12,13]. The ABIC for a given set of $(\lambda, \delta)$ is defined as:

$$ABIC(\lambda,\delta) = (N+P-M)\log(2\pi\hat{\sigma}^2) - P\log\lambda^2 + \log\left|\mathbf{G}(\delta)^{\mathrm{T}}\mathbf{G}(\delta) + \lambda^2\mathbf{L}^{\mathrm{T}}\mathbf{L}\right| - \log\left|\lambda^2\mathbf{L}^{\mathrm{T}}\mathbf{L}\right| + (N+P-M),$$

where $N$ is the total number of gravity data points, $M(=4m)$ is the number of model parameters, and $P$ is the rank of the constraint matrix $\mathbf{L}^{\mathrm{T}}\mathbf{L}$. In this formulation, $\hat{\sigma}^2$ represents the scale factor of the variance, which is estimated from the minimum value of the objective function as:

$$\hat{\sigma}^2 = \frac{U(\widehat{\mathbf{m}})}{N+P-M}$$

We calculated the ABIC values for various combinations of $\lambda$ and $\delta$, selecting the set that minimized the ABIC. Once the optimal hyperparameters $(\lambda_{\mathrm{opt}}, \delta_{\mathrm{opt}})$ and the corresponding variance factor $\hat{\sigma}^2$ are determined, the uncertainty of the estimated model parameters is evaluated. The covariance matrix of the estimation error, $\mathbf{C}_m$, is given by:

$$\mathbf{C}_m = \hat{\sigma}^2\left(\mathbf{G}\left(\delta_{\mathrm{opt}}\right)^{\mathrm{T}}\mathbf{G}\left(\delta_{\mathrm{opt}}\right) + \lambda_{\mathrm{opt}}^2\mathbf{L}^{\mathrm{T}}\mathbf{L}\right)^{-1}$$

The estimation errors (standard deviations) for the density and trend parameters are derived from the square roots of the diagonal elements of $\mathbf{C}_m$.

## 4 Results

### 4.1 Determination of Optimal Hyperparameters

To determine the optimal hyperparameters for the inversion, we performed a grid search over a range of values for the regularization weight $\lambda$ and the structural depth parameter $\delta$. Specifically, we varied $\lambda$ from 200 to 2000 and tested discrete depth values of $\delta$ = 0, 4, 8, and 12 km.

Figure 4 illustrates the variation of ABIC values with respect to $\lambda$ for each depth parameter. The ABIC curves exhibit a distinct convex shape, allowing for a clear identification of the minimum. Among all combinations tested, the global minimum of ABIC was achieved at $\lambda$ = 1000 and $\delta$ = 8 km. Consequently, we adopted these optimal values ($\lambda_{\mathrm{opt}}$ = 1000 and $\delta_{\mathrm{opt}}$ = 8 km) for the subsequent estimation of the density structure and regional VGG trends.

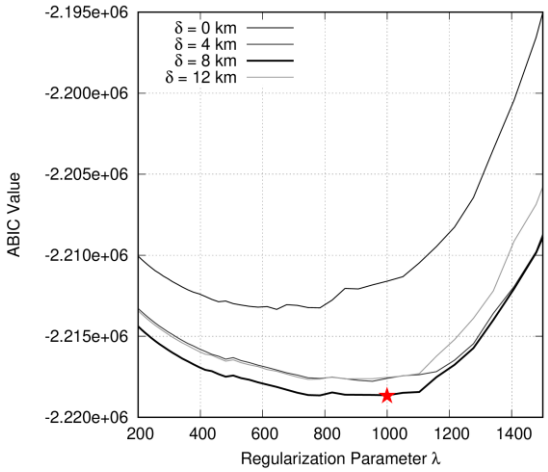


**Figure 4** ABIC values as a function of regularization parameter $\boldsymbol{\lambda}$ and structural depth parameter $\boldsymbol{\delta}$. Star denotes the optimal set of hyperparameters which provides the minimum ABIC.

## 4.2 Surface Density Structure

Figure 5 presents the estimated spatial distribution of the surface density $\rho$, calculated using the optimal hyperparameters. To quantify the statistical characteristics of the estimated model, we also analyzed the frequency distribution of the density values (Figure 5). The histogram exhibits a distribution centered around a mean value of 2760 kg m$^{-3}$ (2.76 g cm$^{-3}$), with a standard deviation of 230 kg m$^{-3}$ (0.23 g cm$^{-3}$). This mean value is in excellent agreement with the standard density of the upper continental crust (2670 kg m$^{-3}$), supporting the physical validity of our inversion results. The distribution is slightly skewed towards the lower density side, reflecting the presence of extensive sedimentary basins.

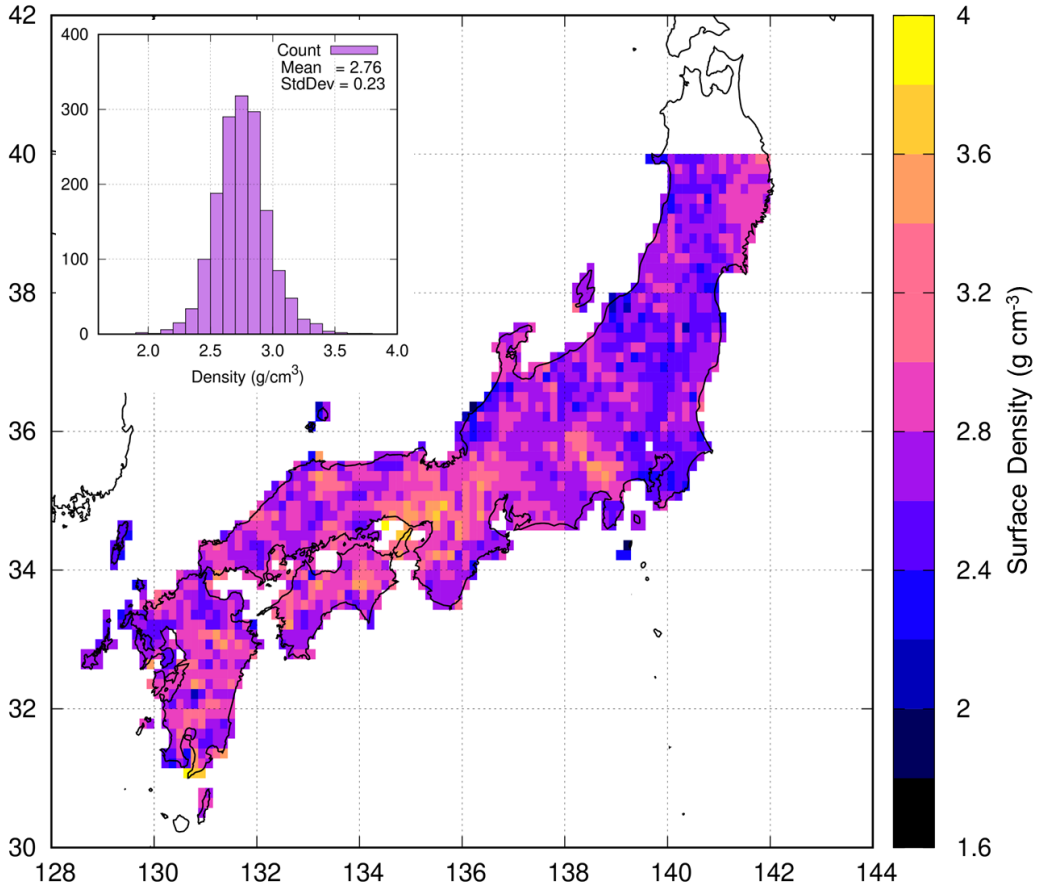


**Figure 5** Spatial distribution of surface density up to 8 km depth, estimated from VGG inversion analysis.

The spatial map (Figure 4) clearly delineates these geological features. Significant low-density zones (approximately 2000-2400 kg $m^{-3}$) are identified in major alluvial plains and sedimentary basins. Specifically, the Kanto Plain exhibits a widespread low-density anomaly, reflecting thick Quaternary sedimentary layers. Similar low-density patterns are observed in the Sendai and Echigo Plains.

In contrast, high-density anomalies, indicated by pink to orange colors (exceeding 2800 kg $m^{-3}$), are dominant in mountainous regions. Notably, the Kitakami and Abukuma Mountains in north-eastern Japan, as well as the mountainous areas of the Kii Peninsula and Shikoku in southwestern Japan, show distinctive high-density signatures. These regions correspond to areas where older basement rocks, such as granites and metamorphic rocks, are exposed or located near the surface.

### 4.3 Regional VGG Trend Model

Figure 6 illustrates the spatial distribution of the estimated regional vertical gravity gradient ($\gamma_{\text{regional}}$). The values predominantly fall within the range of 0.285 to 0.295 mGal m$^{-1}$ (2850-2950 Eötvös), which corresponds to the long-wavelength component of the gravity field possibly originating from deeper crustal structures.

The most striking feature in the map is the distinct linear zone of low VGG values (indicated by blue colors) extending across the central part of the Japanese Islands. This linear anomaly corresponds remarkably well with the western margin of the Fossa Magna, known as the Itoigawa-Shizuoka Tectonic Line (ISTL). The VGG map clearly delineates this major tectonic boundary as a sharp gradient contrast. In addition to Fossa Magna region, another prominent low-VGG anomaly is identified in the Kinki district, Western Japan. This feature suggests the existence of a structural boundary or a tectonic zone with low-density properties in the subsurface, similar to the ISTL.

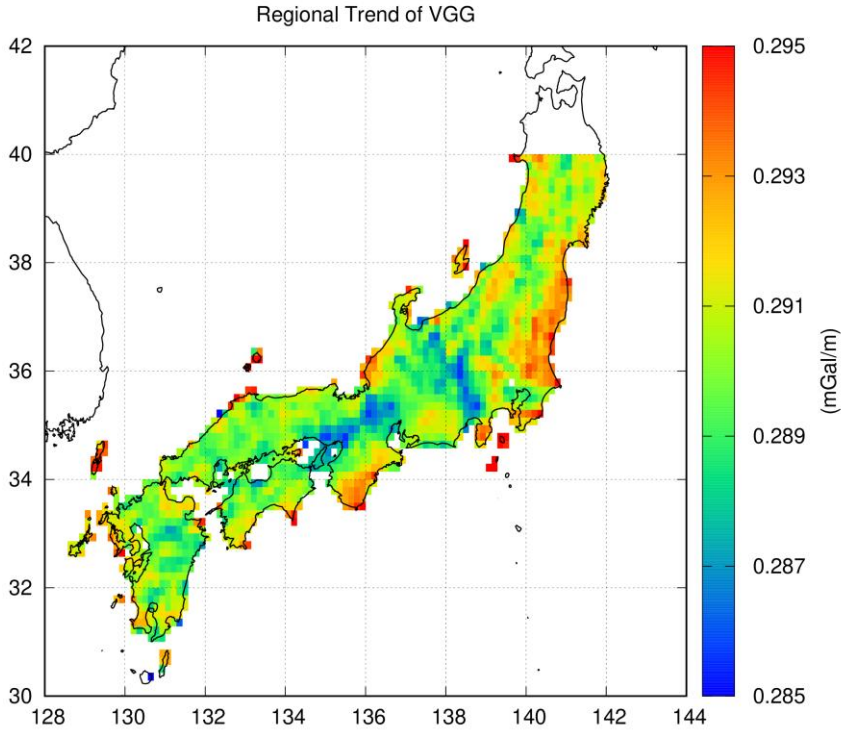


**Figure 6** Regional trend of VGG (Vertical Gravity Gradient) extracted from inversion analysis. The displayed values are $C_k$ terms of the model.

# 5 Discussion

## 5.1 Interpretation of Surface Density Structure

The estimated surface density model shows a strong correlation with the surface geology of the Japanese Islands. The low-density anomalies (2000-2400 kg $m^{-3}$) clearly delineate the distribution of thick Quaternary sediments in major alluvial plains, such as the Kanto, Sendai and Echigo Plains. In contrast, the high-density regions (exceeding 2800 kg $m^{-3}$) correspond to the exposure of pre-Neogene basement rocks, including granites and metamorphic complexes in the Kitakami, Abukuma, and Kii Mountains. This consistency between the gravity-derived density and the geological lithology validates the effectiveness of our VGG inversion method.

Comparison with the terrain density estimation by Nawa et al. (1997) [1] highlights the advantage of our approach. Nawa et al. (1997) estimated average crustal densities in Western Japan by exploiting the correlation between surface gravity anomalies and topography. Their results show a density distribution in mountainous areas that is generally consistent with our findings. However, their method inherently struggled to determine densities in flat regions with little topographic relief, such as the Nobi and Osaka Plains, due to the lack of correlation between gravity and topography.

In contrast, the present study successfully estimated surface densities even in these flat alluvial plains. This success is attributed to two key factors. First, the use of VGG effectively emphasizes short-wavelength components of the gravity field, making the signals from shallow density contrasts (e.g., sedimentary basins) distinct from deep-seated regional trends. Second, our inversion scheme models the regional VGG trend by imposing a continuity constraint across the analysis grid. This regularization stabilizes the separation of the regional trend from the local density signals, allowing for robust density estimation even in areas where topographic relief is minimal.

## 5.2 Tectonic Implications of VGG Trends

The regional VGG map (Figure 6) provides critical insights into the tectonic framework of Central Japan, particularly regarding the Fossa Magna Tectonic Zone. The most prominent feature is the sharp low-VGG belt along the western margin, corresponding to the Itoigawa-Shizuoka Tectonic Line (ISTL). This distinct gradient suggests that the density boundary at the ISTL is structurally sharp and extends vertically to a considerable depth. We also note a linear low-VGG trend

extending from Osaka Plain to the Lake Biwa region in Western Japan, which implies a structural connectivity of the sedimentary basins in the Kinki district.

While the western margin (ISTL) is clearly defined, the eastern margin of the Fossa Magna is less distinct in the raw regional VGG map. This ambiguity arises because high-density pre Quaternary formations (e.g., the Kanto Mountains) produce positive VGG anomalies that mask the signal from the deeper rift structure. To overcome this, we applied a geological mask to exclude regions dominated by pre-Quaternary rock exposures (Figure 7), thereby focusing on the VGG signature of the younger sedimentary fill. The masked VGG map reveals a broad low-VGG zone, exceeding 100 km in width, extending across Central Japan. The eastern boundary of this low-VGG zone aligns remarkably well with the Kashiwazaki-Chiba Line and the Shibata-Koide Line (Yamashita, 1995 [14]; Takahashi 2006 [15]). These results support the geological hypothesis that the Fossa Magna is a wide rift basin bounded by these tectonic lines, rather than a simple narrow boundary.

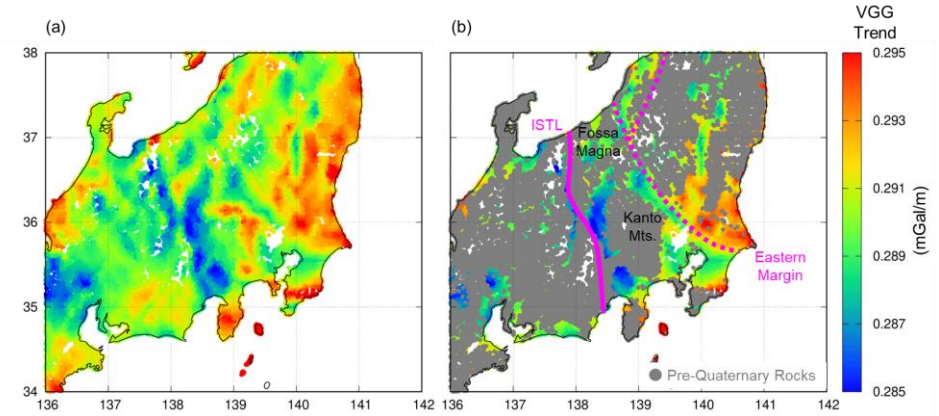


**Figure 7** Regional vertical gravity gradient (VGG) trends highlighting the Fossa Magna structure. (a) The spatial distribution of the regional VGG trend ($\gamma_{\mathbf{regional}}$) obtained from the inversion analysis. High VGG anomalies are observed in mountain range such as the Kanto Mountains. (b) The VGG trend map masked by surface geology. Areas of pre-Quaternary rock exposures are masked in gray to highlight gravitational signature of thick sedimentary basins. The broad low-VGG zone (blue to light green) clearly delineates the Fossa Magna rift basin. The solid magenta line indicates the Itoigawa-Shizuoka Tectonic Line (ISTL), marking the western boundary. The dashed magenta line indicates the proposed Eastern Margin (corresponding to the Kashiwazaki-Chiba Line and Shibata-Koide Line).

## 5.3 Comparison with Seismic Velocity Model

Finally, we verified the reliability of our estimated density structure by comparing it with independent S-wave velocity (Vs) models. We utilized two representative 3-D velocity models of the Japanese Islands: (1) the body-wave tomography model by Matsubara et al. (2022) [16], and (2) the ambient noise surface-wave tomography model by Nishida et al. (2008) [17]. We calculated the Pearson correlation coefficients between our estimated surface density values and the Vs values extracted at various depths from these models.

The calculated correlation coefficients are summarized as follows:

- **Comparison with Matsubara et al. (2022)**: 0.133 at 6 km depth, 0.144 at 10 km depth
- **Comparison with Nishida et al. (2008)**: 0.114 (2 km), 0.099 (4 km), **0.228 (6 km)**, 0.146 (8 km), and 0.180 (10 km)

Although the correlation coefficients are not strongly high overall, they consistently exhibit positive values. This positive correlation is physically reasonable, as denser rocks generally possess high shear moduli and thus higher seismic velocities. Notably, the highest correlation (R = 0.228) was observed with the Nishida model at a depth of 6 km (Figure 8). This depth corresponds to the mid-to-lower part of the density contrast layer assumed in our inversion ($\delta_{opt}$ = 8 km). Since our VGG inversion estimates a vertically averaged density for the upper 8 km, it is reasonable that the result correlates best with the seismic structure at an intermediate depth (around 6 km) rather than at very shallow (2-4 km) or deeper (> 10 km) levels.

The moderate correlation values can be attributed to the different physical sensitivities of the methods. Seismic velocity is strongly affected by pore fluids and microfractures, particularly in the shallow crust, which may reduce velocity without significantly altering bulk density. Furthermore, the VGG method resolves density contrasts based on the integrated vertical gradient, which inherently results in a smoother structural image compared to the high-resolution heterogeneity captured by body-wave tomography. Nevertheless, the statistically significant correlation at 6 km depth with the surface-wave model, which also captures broader crustal features, supports the validity of our estimated density distribution as a representation of the average upper crustal structure.

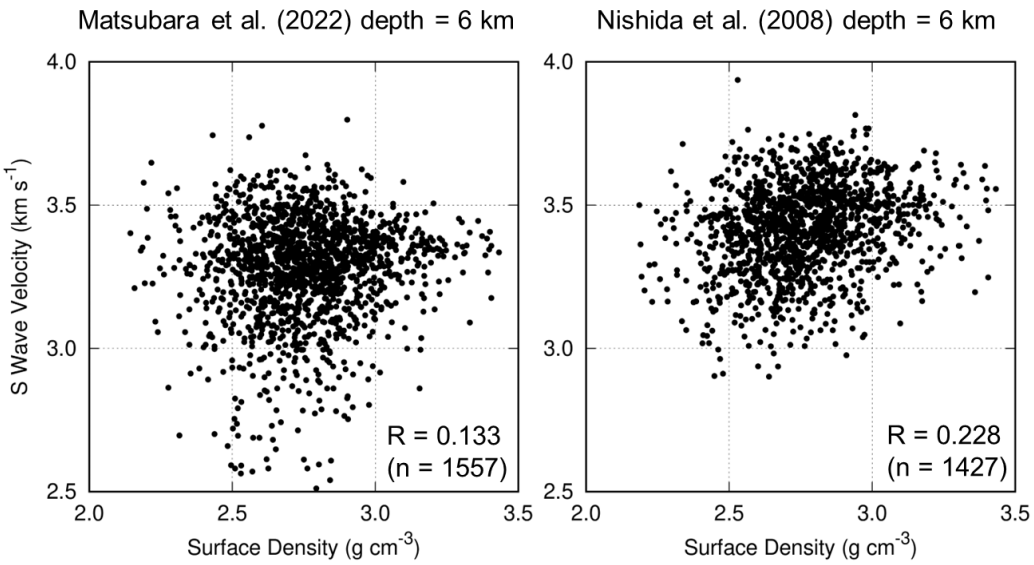


**Figure 8** Comparison between surface density and seismic S-wave velocity models (left: body wave tomography model by Matsubara et al., 2022, right: surface wave tomography model by Nishida et al., 2008).

# 6 Conclusions

We successfully estimated the near-surface density structure and regional vertical gravity gradient (VGG) trends in Central and Western Japan by inverting the difference between terrestrial and airborne gravity data. The estimated surface density shows an excellent agreement with surface geology, accurately resolving low-density sedimentary basins even in flat terrains where conventional methods often fail, and exhibits a moderate positive correlation with seismic velocity models. The regional VGG trend clearly delineates the Itoigawa-Shizuoka Tectonic Line and reveals a significant low-VGG lineament extending from Osaka Plain to Lake Biwa. Furthermore, regarding the Fossa Magna's eastern margin, our masking analysis supports the wide-rift hypothesis bounded by the Kashiwazaki-Chiba and Shibata-Koide Lines. We conclude that this VGG approach is a powerful tool for visualizing upper crustal tectonics, offering superior resolution to conventional Bouguer anomaly analysis.

## Data Availability

Publicly available datasets were analyzed in this study. The raw gravity data can be accessed from the respective databases cited in the text. The derived data (terrestrial-airborne gravity pairs) supporting the findings of this study are available from the corresponding author upon reasonable request.

## Acknowledgements

We used terrestrial and airborne gravity data and the geoid model provided by the Geospatial Information Authority of Japan (GSI). We also utilized gravity data from the National Institute of Advanced Industrial Science and Technology (AIST), Kanazawa University, the Gravity Database of Southwest Japan, and the Gravity Database of Japan. We express our sincere gratitude to all the researchers and engineers who dedicated themselves to the monumental effort of acquiring and compiling these valuable datasets.

## References

[1] Nawa, K., Y. Fukao, R. Shichi, and Y. Murata (1997). Inversion of gravity data to determine the terrain density distribution in southwest Japan, *J. Geophys. Res.*, **102**(B12), 27703–27719, doi:10.1029/97JB02543

[2] Geospatial Information Authority of Japan (2024). JGSN2016 Terrestrial Gravity Data, https://www.gsi.go.jp/common/000275020.zip

[3] Geological Survey of Japan, AIST (2013). Gravity Database of Japan, DVD edition https://www.gsj.jp/Map/JP/geophysics3.html

[4] Honda, R., A. Sawada, N. Furuse, T. Kudo, T. Tanaka, and Y. Hiramatsu (2012). Release of Gravity Database of the Kanazawa University, *Journal of the Geodetic Society of Japan*, **58**(4), 153-160, https://doi.org/10.11366/sokuchi.58.153 (In Japanese with English abstract)

[5] Gravity Research Group in Southwest Japan (2001). Gravity Database of Southwest Japan (CD-ROM), Bulletin of the Nagoya University Museum, Special report, No. 9.

[6] Yamamoto, A., R. Shichi, and T. Kudo (2011). Gravity Database of Japan (CD-ROM), Chubu

University, Special Publication, No. 2.

[7] Geospatial Information Authority of Japan (2024). Airborne gravity data, https://www.gsi.go.jp/butsuri/data/AirborneGravity_zenkoku.zip

[8] Geospatial Information Authority of Japan (2025). Geoid 2024 Japan and its surroundings, Trial Version, https://www.gsi.go.jp/butsuri/data/manual_GSIGEO2024beta.pdf (in Japanese)

[9] European Space Agency (2024). *Copernicus Global Digital Elevation Model*. Distributed byOpenTopography. https://doi.org/10.5069/G9028PQB

[10] GEBCO Compilation Group (2024). GEBCO 2024 Grid, https://doi.org/10.5285/1c44ce99-0a0d-5f4f-e063-7086abc0ea0f

[11] Hofmann-Wellenhof, B., and H. Moritz (2006). Physical Geodesy second edition, Springer, https://doi.org/10.1007/978-3-211-33545-1

[12] Akaike, H. (1980). Likelihood and the Bayes procedure. In J. M. Bernardo, M. H. DeGroot, D. V. Lindley, & A. F. M. Smith (Eds.), *Bayesian Statistics* (pp. 143–166). Valencia, Spain: University Press.

[13] Okazaki, T., Fukahata, Y., and Nishimura, T. (2021). Consistent estimation of strain-rate fields from GNSS velocity data using basis function expansion with ABIC. *Earth Planets Space* **73**, 153. https://doi.org/10.1186/s40623-021-01474-5

[14] Yamashita, N. (Ed.) (1995). *Fossa Magna* (in Japanese), 310 pp., Tokai Univ. Press, Tokyo.

[15] Takahashi, M. (2006). Tectonic boundary between Northeast and Southwest Japan Arcs during Japan Sea opening. Journal of the Geological Society of Japan, 112, 14-32. (in Japanese with English abstract) https://doi.org/10.5575/geosoc.112.14

[16] Matsubara, M., Ishiyama, T., No, T. et al. (2022), Seismic velocity structure along the Sea of Japan with large events derived from seismic tomography for whole Japanese Islands including reflection survey data and NIED MOWLAS Hi-net and S-net data. *Earth Planets Space* 74, 171. https://doi.org/10.1186/s40623-022-01724-0

[17] Nishida, K., H. Kawakatsu, and K. Obara (2008), Three-dimensional crustal *S* wave

velocity structure in Japan using microseismic data recorded by Hi-net tiltmeters, *J. Geophys. Res.*, 113, B10302, doi:10.1029/2007JB005395